

Assessment of Arterial Reflection Markers using an A-Mode Ultrasound Device

Rahul Manoj
Department of Electrical Engineering
Indian Institute of Technology Madras
Chennai, India
rahul_manoj@smail.iitm.ac.in

Raj Kiran V
Department of Electrical Engineering
Indian Institute of Technology Madras
Chennai, India
ee15d020@smail.iitm.ac.in

Nabeel PM
Healthcare Technology Innovation
Centre (HTIC), IIT Madras
Chennai, India
nabeel@htic.iitm.ac.in

Mohanasankar Sivaprakasam
Department of Electrical Engineering
Indian Institute of Technology Madras
Chennai, India
mohan@ee.iitm.ac.in

Jayaraj Joseph
Department of Electrical Engineering
Indian Institute of Technology Madras
Chennai, India
jayaraj@ee.iitm.ac.in

Abstract— Reflections of arterial blood pulse waves have a pivotal role in the equilibrium of the vasculature. Elevated levels of wave reflections cause an increase in pulse pressure and pulse propagating speeds, exacerbating cardiovascular risk. Quantification of reflection markers is either based on augmentation index or reflection magnitude (RM) and reflection index (RI), both derived from wave separation analysis (WSA). Simultaneous measurement of pressure and flow velocity from the same arterial site is a requirement for WSA and has its practical challenges. Subsequently, simplified WSA based on modelling flow is proposed. This work explores the feasibility of using multi-Gaussian decomposition (MGD) of diameter scaled pressure waveform to perform a WSA and quantify the reflection markers. The diameter waveforms are obtained using an A-mode ultrasound device (ARTSENS®). The decomposed pressure signals scaled from diameter waveforms (or Gaussians) are uniquely combined to yield a forward and backward wave. The reflection markers derived from MGD based WSA are then compared with the clinically relevant stiffness markers and with age. The study was conducted on 110 healthy subjects (60 males and 50 females). A moderately significant correlation ($r > 0.51$, $p < 0.001$) was obtained for RM and RI when compared with stiffness markers (β , E_p , AC, PWV and AIx). The highest correlation was observed for RM versus E_p ($r = 0.602$, $p < 0.001$), followed by β and PWV. The correlation in reflection markers with age was captured with $r = 0.51$, $p < 0.001$. A change of 25.2% and 15.4% were observed for the group average RM and RI, respectively, among normotensive and hypertensive subjects in this cohort. The proposed MGD model has the potential to explore the central arterial biomechanics from a diameter or pressure waveform. The variations in reflection markers with stiffness and age derived using the proposed WSA approach were faithfully captured. The flow-independent WSA, combined with a field-deployable measurement device like ARTSENS®, has the potential to conduct large scale vascular screenings in a resource-limited setting.

Keywords—Gaussians, reflection magnitude, reflection index, arterial stiffness, pulse wave velocity, carotid artery, vascular ageing, ultrasound, diameter, reflection, augmentation index

I. INTRODUCTION

Reflection of pulse waves occurs due to mismatches in the intrinsic impedance of blood vessels. The structural and functional properties of blood vessels are interlinked with its impedance. Any change in the impedance, partly due to geometry (branching, tapering), material property (stiffness, stiffens gradient) and peripheral resistance, will cause reflections and re-reflections of arterial pulse waves [1].

Therefore, pressure and flow velocity measured at any arterial site is a superposition of a forward wave ejected from the heart and a backward wave (comprising reflections and re-reflections) returning to the heart.

Wave reflections determine the morphology of the pulse waves, contributing to the rise in systolic and pulse pressure in both elastic and muscular arteries. They become more significant with increasing biological age and in patients with hypertension [2]. Elevated wave reflections are associated with evidence of increased ventricular workload, incident heart failure [3], exacerbating cardiovascular risk and all-cause mortality [4]. There is a shift away from the classical strategy relying solely on the reduction of blood pressure (BP) values in the anti-hypertensive treatment to include reduction in arterial stiffness, wave reflection and pulse pressure as a treatment strategy. Quantification of reflection in terms of reflection markers can therefore serve as a therapeutic goal in hypertension management [5]. Reflection markers will include Reflection Magnitude (RM), defined as the ratio between pulse pressure of backward wave (ΔP_B) to that of forward wave (ΔP_F), and Reflection Index (RI) defined as the ratio of ΔP_B expressed as a percentage of total pulse pressure of forward and backward waves ($\Delta P_F + \Delta P_B$).

The commonly used tool to quantify reflection is the Augmentation Index (AIx), which lacks a strong prognostic value due to the influence of many confounding factors [6]. More advanced unequivocal wave separation analysis (WSA) exists that requires simultaneously measured pressure and flow velocity information (ideally from the same arterial site) to separate the forward-backward components and to quantify the reflection markers; namely, impedance analysis [7] and wave intensity analysis (WIA) [8]. The former method consists of decomposing the pressure and flow velocity waves in the frequency domain, and the approach is only valid in a linear system requiring complex Fourier analysis. The latter approach (WIA) decomposes the waves into successive wavefronts in the time domain, overcomes the restrictions imposed in the impedance analysis, but is highly susceptible to noise [9]. It is important to note that the synchronized, simultaneous acquisition of pressure and flow velocity from an arterial site has its practical challenges [10], [11]. Subsequently, simplified WSA methods have been proposed by modelling required flow velocity waveforms from the measured pressure wave [12]–[14].

TABLE I Mathematical expression for clinically relevant stiffness markers

Stiffness Marker	Expression
Elastic modulus (Peterson) (kPa)	$E_p = \frac{\Delta P}{\Delta D/D}$
Specific Stiffness, β	$\beta = \frac{\ln(\frac{P_s}{P_d})}{\Delta D/D}$
Pulse Wave Velocity (m/s)	$PWV = \sqrt{\frac{D_D}{2\rho} \times \frac{\Delta P}{\Delta D}}$
Arterial Compliance (mm ² /kPa)	$AC = \frac{\pi(D_s^2 - D_d^2)}{4\Delta P}$
Augmentation Index (%)	$\frac{\text{Augmented Pressure}}{\text{Pulse Pressure}} \times 100$

In this work, we demonstrate the i) feasibility of quantifying reflection markers (RM and RI) using a WSA based on multi-Gaussian decomposition (MGD) of pressure wave scaled from diameter waveforms and ii) compare the agreement of reflection markers with clinically relevant stiffness markers (See TABLE I for description) and with age. The diameter waveforms and stiffness markers are obtained in a field setting using the extensively validated image free (A-Mode) ultrasound device ARTSENS® [15], [16]. The theory and measurement protocol are described in the subsequent sections, followed by results and observations accompanying insights to future research.

II. MATERIALS AND METHODS

A. Theory of MGD Modelled Wave Separation Analysis

The forward ($P_F(t)$) and backward wave ($P_B(t)$) are separated from the pressure wave $P(t)$, as

$$P_F(t) = \frac{1}{2}(P(t) + U(t) \times Z_c) \quad (1)$$

$$\text{and, } P_B(t) = \frac{1}{2}(P(t) - U(t) \times Z_c), \quad (2)$$

where $U(t)$ is blood flow velocity and Z_c is the magnitude of the characteristic impedance of the blood vessel [17].

When $P(t)$ is represented as a sum of two functions, say $G_1(t)$ and $G_2(t)$, it gives:

$$P(t) = G_1(t) + G_2(t) \quad (3)$$

$$\text{such that, } G_1(t) = U(t) \times Z_c \quad (4)$$

$$\text{and } G_2(t) = P(t) - (U(t) \times Z_c) \quad (5)$$

By substituting (4) and (5) in (1) and (2), an expression for $P_F(t)$ and $P_B(t)$ can be written as:

$$P_B(t) = \frac{G_2(t)}{2} \quad (6)$$

$$\text{and } P_F(t) = G_1(t) + \frac{G_2(t)}{2} \quad (7)$$

The MGD modelled WSA decomposes the arterial pressure waveform into a sum of N Gaussian functions,

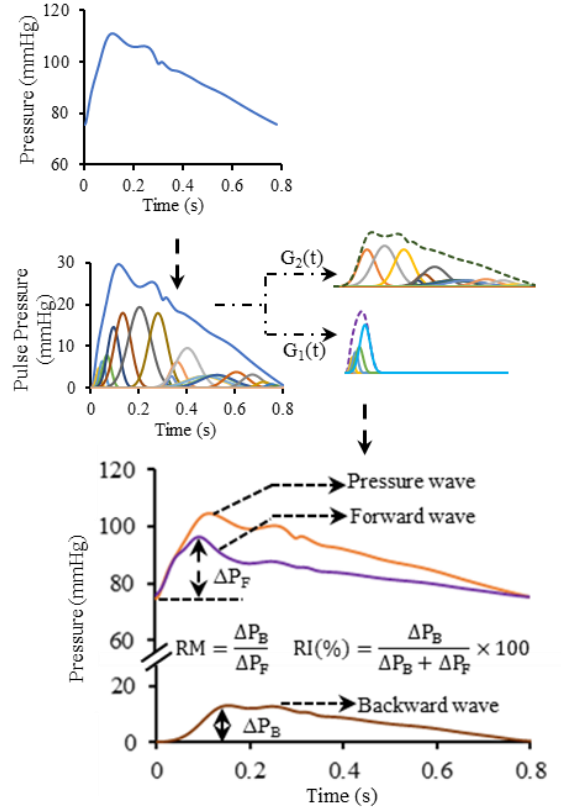


Fig.1 Wave separation analysis using multi-Gaussian decomposition of pressure waveform

which are uniquely combined to yield $G_1(t)$ and $G_2(t)$ [18]. Fig.1 illustrates the overall MGD modelling of a pressure waveform. A Gaussian wave or its linear combination is a rational way of representing a pulse wave with a small set of parameters. This could be a potential solution to understanding the confluence of reflections waves. Till date, multi-Gaussian modelling of pulse waves was limited to merely establishing an epidemiological relation of shifts in Gaussian curves in terms of reflection quantification indices [19]. Of the ' N ' Gaussians that decompose the pressure waveform, $G_1(t)$ is obtained from the first ' n ' among the Gaussians (when sorted by the ascending time-positions) that exist till the dicrotic notch of $P(t)$. Further, $G_2(t)$ is constructed from the remaining ' $N - n$ ' Gaussians.

$$G_1(t) = \sum_{i=1}^n g_i(t) \quad (8)$$

$$\text{and } G_2(t) = \sum_{i=n+1}^N g_i(t), \quad (9)$$

$$\text{where, } g_i(t) = A_i e^{-\frac{1}{2} \times \frac{(t-M_i)^2}{C_i^2}}. \quad (10)$$

In (10), A_i is the amplitude or weight, M_i is the mean locations, and C_i is the standard deviation from M_i for the respective Gaussian $g_i(t)$. The MGD-modelled pressure waveform $\hat{P}(t; K)$ is obtained by performing a non-linear curve fit optimization using Levenberg-Marquardt (LM) algorithm on $P(t)$. The LM algorithm optimizes the parameters ($K_i: A_i, M_i, C_i$) for a given N , by minimizing the

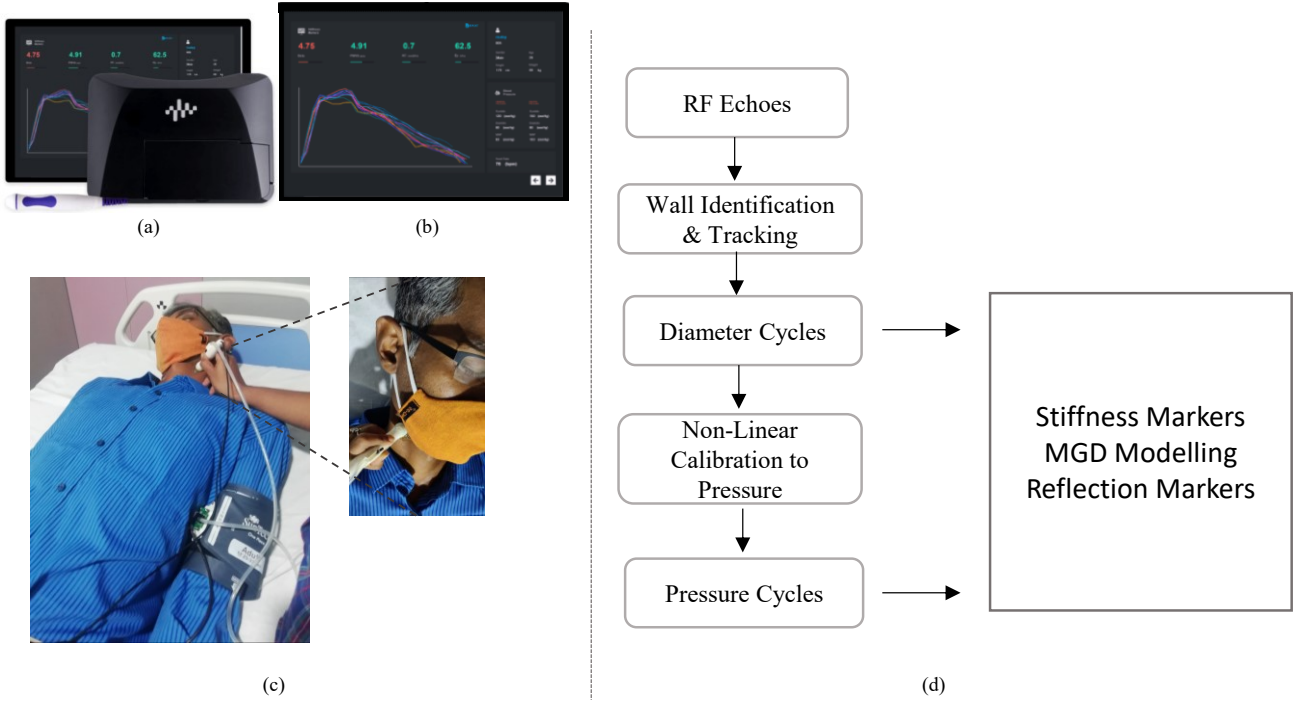


Fig.2 (a) Device illustration showcasing the probe, hardware, and GUI, (b) GUI on a Windows 10 Tablet (c) ARTSENS probe positioning at carotid artery at supine position, (d) Flow chart of the architecture

weighted (W_j) sum of the squares of errors (χ^2) between ($\hat{P}(t; K)$) and $P(t)$ as,

$$\chi^2 = \sum_{j=1}^m W_j \left(P(j) - \hat{P}(j; K) \right)^2 = \sum_{j=1}^m W_j \left(P(j) - \sum_{i=1}^N g_i(j) \right)^2 \quad (11)$$

A parametric analysis in a previous study was performed by iteratively varying (N, n) within fixed boundaries for the study cohort. The model designed from these combinations of (N, n) for each type of waveform morphology (Type-A, type-B and Type-C) were applied in this study.

B. A-Mode Ultrasound Device

The instrument used in this study consists of a custom-made A-Mode ultrasound transducer (single channel), with a centre frequency of 5 MHz, 1.3-degree spatial angle, 360 μm axial resolution, 5 mm in diameter, embedded in a 3D printed, ergonomically designed probe. The excitation and acquisition hardware consists of a pulser-receiver IC (STHV 748, STM Electronics), which isolates the ultrasound transducer with a $\pm 40\text{V}$, 200 ns time period high voltage pulse train. The digital logic required for STHV748 are controlled via a 32-bit ARM Cortex M4 (LPC4370FET256, NXP Semiconductors) microcontroller. The LPC4370FET256 will generate the logic to switch between the transmit and receive states at a frame rate of 40 Hz. A scan depth of 40 mm depth, equivalent to 52 μs of Radio Frequency (RF) signals, are acquired at a sampling rate of 80 MHz, using a high-speed 12-bit ADC of LPC4370FET256. The instrument is powered via USB and runs on a Windows[®] 10 tablet. To perform an arterial diameter measurement, the probe needs to be positioned normal to the pulsating artery to capture the sharpest RF echoes. Poor off-axis sensitivity along with a narrow spatial angle ensures measurements are performed along with the diameter of the artery. This ultrasound hardware circuit is the latest version of the ARTSENS[®] technology [20], [21]. Fig.2

depicts the measurement on a subject using ARTSENS[®], and the device.

C. Data Processing

The algorithm to convert the A-scan RF echoes to diameter waveform is extensively validated [22]. The automated algorithms of ARTSENS[®] identify the near and far walls and continuously tracks them to determine the lumen diameter. LabVIEW based application is used to process the digitized RF echoes. A 4th order zero-phase bandpass filter with a lower cut-off frequency of 1 MHz and higher cut-off frequency of 8 MHz is applied to the RF frames. A time-varying gain to compensate for signal attenuation due to tissue layers were applied with an attenuation coefficient assumed to be 0.7dB/cm/MHz. The obtained diameter waveform was converted to pressure waveform for the carotid artery using an exponential relationship between pressure and arterial cross-sectional area, as in (12),

$$P(t) = P_D e^{\alpha(A(t)/A_D - 1)} \quad (12)$$

where, $P(t)$ is the obtained pressure waveform, P_D is the diastolic BP value, α is the rigidity constant, $A(t)$ is the cross-sectional area waveform, and A_D is the end-diastolic area. The pressure waveform was then calibrated with diastolic blood pressure and mean arterial pressure, obtained via oscillometric BP device at brachial artery by iteratively varying the rigidity constant used in the empirical relationship [23]. The obtained pressure and diameter waveform was used to calculate the stiffness markers (E_p , β , PWV, AC, AIX). Automated processing of the MGD modelled WSA based on the pressure waveform obtained, and the calculation of reflection markers (RM and RI) were implemented using LabVIEW[®].

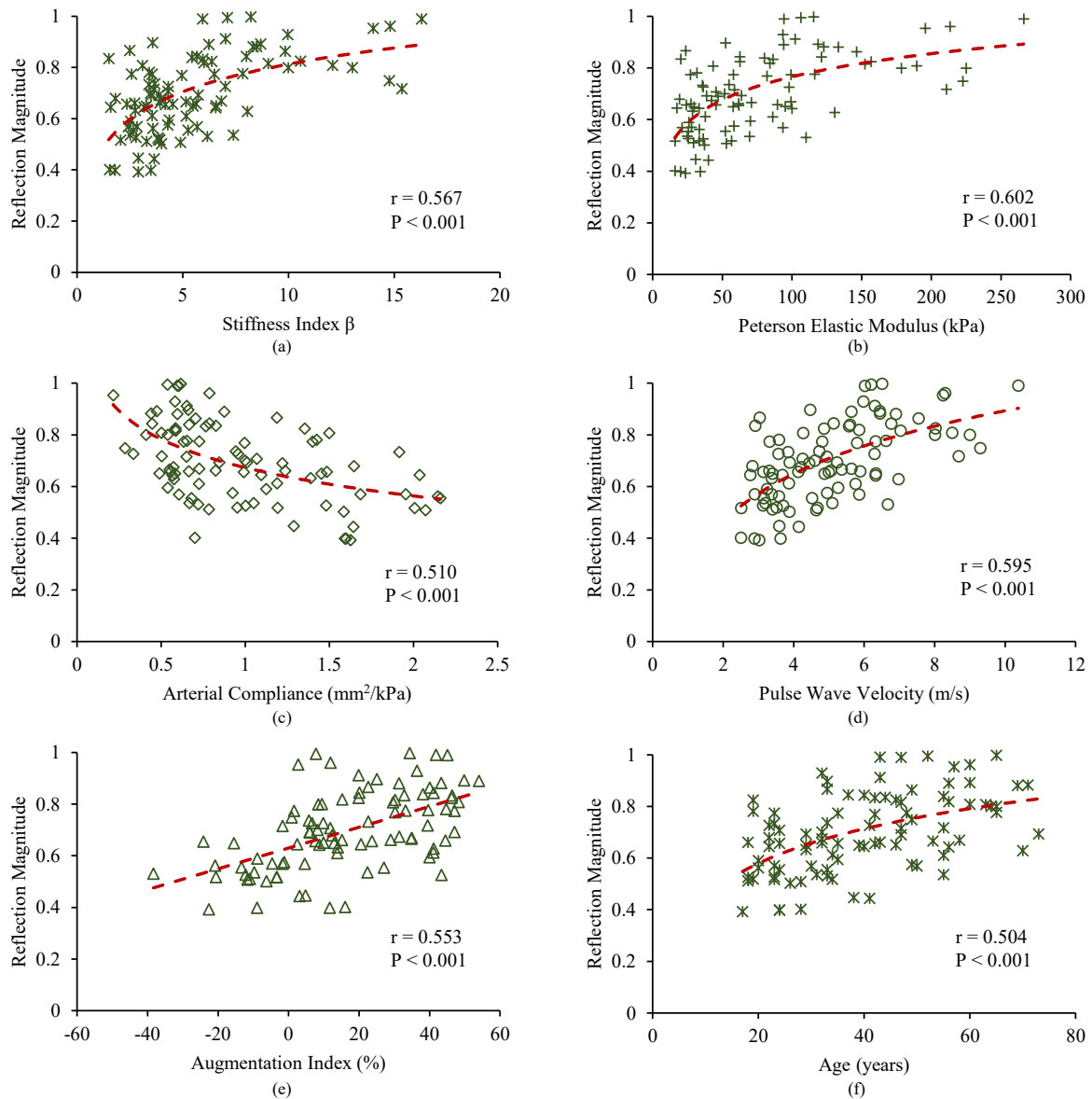


Fig.3. (a)-(e) Correlation of reflection markers (RM) with stiffness markers, (f) correlation plot for RM with age

D. Study Population & Measurement Protocol

The observational study consisted of 50 female and 60 male participants ($n=110$), conducted at a multi-specialty hospital in Chennai, India (VHS-IEC/17-2016). Basic information on the participants, such as age, gender, medications, diet, sleep cycle, physical activities, smoking and alcohol consumption, were collected; along with their written consent in accordance with World Medical Association Declaration of Helsinki: Ethical principles for medical research involving human subjects, revised in 2013, to voluntarily participate in this study. Study participants were familiarized with the study protocols, devices used, and the environment. Basic anthropometry measurements such as height and weight were measured. The subjects were then relaxed for 10 mins in the supine position before the ultrasound and BP measurement. A total of two trials were performed for all study participants. The BP is measured using a clinical-grade automated cuff based oscillometric device on the left arm, at the brachial artery site prior and after the ultrasound measurement. The average BP values are

then used for assessment. ARTSENS[®] measurement is followed by the BP measurement.

E. Statistical Analysis

Results obtained from time-series data; continuous variables are reported as mean \pm standard deviation. To compare the correlation and statistical significance, a regression analysis was performed between the reflection markers such as RM and RI, with stiffness markers and age. Linear and logarithmic correlation (reported in r -value) and curve fit was obtained, and statistical significance was reported in p -value. The similarity/difference between hypertensive and normotensive population based on RM and RI was presented using box-whisker plots constructed using median and interquartile ranges. The level of significance of $\alpha = 0.05$ was used in all the test, and a $p < 0.05$, confirmed statistical significance.

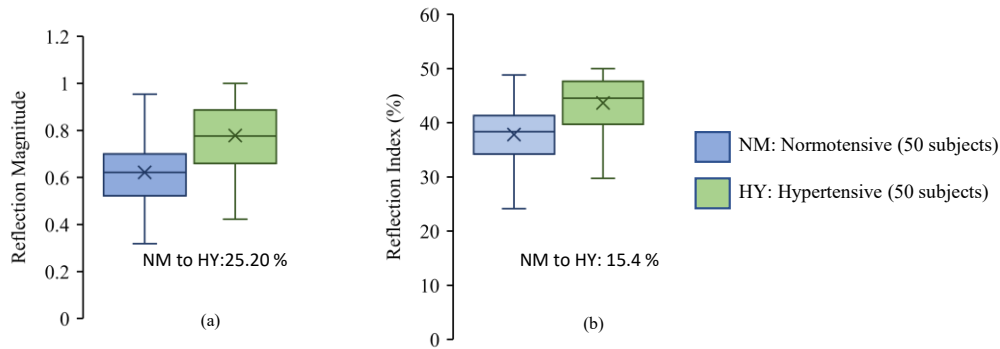


Fig.4 (a) Group average-based classification ($p < 0.05$) of normotensive and hypertensive subjects based on RM and (b) Group average-based Classification ($p < 0.05$) of normotensive and hypertensive subjects based on RI

III. RESULTS AND DISCUSSION

A. Subject Demography

The mean age of 110 subjects (60 male and 50 female) was 49 ± 12 years. The systolic BP varied from 94 mmHg to 208 mmHg, and diastolic BP ranged from 75 mmHg to 115 mmHg. The number of normotensive subjects was 55, and hypertensive was 55. The range of β , Ep, AC, PWV and AIX for this study population varied from 1.44-15.35, 16.08-275.45 (kPa), 0.21-2.18 (mm^2/kPa) and 2.50-11.22 (m/s) and -40% to +55% respectively.

B. Reliability of Signals

The digitized RF frames were recorded with a SNR > 25 dB. The RF echoes capture the left carotid artery wall dynamics and undergo real-time processing to obtain high fidelity diameter waveform. Thus, obtained diameter signals were continuous and quasi-periodic. Comparing all the subjects, the average end-diastolic diameter was 5.63 ± 1.89 mm, and the average distension was 0.58 ± 0.38 mm. The algorithms were able to classify the pressure waveforms (derived from diameter) into Type-A, Type-B and Type-C groups needed for implementing MGD based WSA.

C. Agreement of Reflection Markers with Stiffness Markers

Group average RM and RI for the study cohort were 0.69 ± 0.16 and 40.73 ± 6.11 %. A statistically significant moderate correlation ($r > 0.51$, $p < 0.001$) was obtained between reflection markers (RM, RI) and clinically relevant stiffness markers (β , Ep, AC, PWV and AIX). The correlation plots for RM and stiffness markers are depicted in Fig. 3. There exists a logarithmic trendline between reflection markers and stiffness markers, among which Ep had the highest correlation with RM ($r = 0.602$, $p < 0.001$), followed by PWV ($r = 0.595$, $p < 0.001$), β and AIX ($r > 0.55$, $p < 0.001$). AC had a decreasing trendline with RM and the poorest correlation ($r = 0.510$, $p < 0.001$) among all the stiffness markers. The obtained relationships are at par with the trendlines reported in the literature.

Stiffness markers of the artery are a measure of arterial compliance or distensibility and its surrogates. Changes in the arterial compliance under a distending pressure create changes in the impedance of the blood vessel creating a recoil effect for the forward pressure and flow wave. It is the Windkessel effect (which relies on the elastic properties of the artery) that enables the recoil and acts as a buffering chamber. An increase in stiffness will amplify pulse

propagation speed (or PWV), causing the peripheral reflection wave to augment the systolic blood pressure and afterload. This effect was faithfully captured in the trends obtained.

D. Agreement of Reflection Markers with Age

A statistically significant and moderate correlation ($r > 0.504$, $p < 0.001$) was observed between reflection markers (RM and RI) and age. The correlation plot for RM versus age is depicted in Fig. 3(f). Similar trendlines were reported in the literature [24]. As age increases, the arteries tend to get stiffer, and there is disappearance or reversal of the elastic/stiffness gradient from central arteries to peripheral arteries (the central arterial stiffness increases to a value closer to the peripheral arterial stiffness with age) [25], [26]. This causes impedance mismatch point to shift towards the central arteries, an increase in pulse pressure and reflections to appear early, resulting in elevated levels of reflection markers.

E. Normotensive and Hypertensive Classification

The group average RM and RI for normotensive (SBP < 120 mmHg and DBP < 80 mmHg) population was 0.65 ± 0.19 and 37.81 ± 5.66 % respectively. Similarly, for hypertensive (SBP > 140 mmHg and DBP > 90 mmHg) population it was 0.77 ± 0.14 and 43.64 ± 5.12 % respectively. A change of 25.2% and 15.4% was observed between the group average RM and RI of the normotensive and hypertensive population, as depicted in Fig. 4.

Conventional hypertension treatment methods monitor reductions in DBP and SBP levels. However, it is increasingly crucial to include reductions in carotid pulse pressure [27], arterial stiffness, pulse wave velocity [28] and its incremental change within a cardiac cycle [29], and the extent of wave reflections as part of devising treatment strategies. Cardiovascular events and associated risks are largely influenced by the pulsatile nature of the blood than the steady-state components. The rise of wearable platforms enables continuous monitoring of ECG [30], [31], heart rate [32], respiratory rate [33], [34], when combined with pulsatile blood markers as part of anti-hypertensive treatment strategies, shifting focus from conventional markers, as integral goals of drug based therapy [5].

IV. CONCLUSION

In this work, we have presented the feasibility of using multi-Gaussian decomposition of diameter scaled pressure

waveform for carotid artery and hence to perform a WSA. The diameter signals were acquired using the most evolved version of our image free ultrasound device called ARTSENS®. The obtained reflection markers (RM and RI) from forward-backward WSA were compared with clinically relevant stiffness markers (β , Ep, AC, PWV and AIx) and with age. There existed a moderate and statistically significant correlation between both reflection markers. They were further used to group normotensive and hypertensive subjects among the study population. The MGD based WSA on diameter scaled pressure waveforms has enabled quantification of reflection markers without the need for any measured or modelled flow measurements. The practical advantage of using ARTSENS® technology helps perform large-scale vascular screenings in resource-limited settings.

REFERENCES

- [1] J. P. Mynard, A. Kondiboyina, R. Kowalski, M. M. H. Cheung, and J. J. Smolich, "Measurement, Analysis and Interpretation of Pressure/Flow Waves in Blood Vessels," *Front. Physiol.*, vol. 11, no. August, pp. 1–26, 2020.
- [2] C. Manisty *et al.*, "Wave Reflection Predicts Cardiovascular Events in Hypertensive Individuals Independent of Blood Pressure and Other Cardiovascular Risk Factors. An ASCOT (Anglo-Scandinavian Cardiac Outcome Trial) Substudy," *J. Am. Coll. Cardiol.*, vol. 56, no. 1, pp. 24–30, 2010.
- [3] P. Zamani *et al.*, "Pulsatile Load Components, Resistive Load and Incident Heart Failure: The Multi-Ethnic Study of Atherosclerosis (MESA)," *J. Card. Fail.*, vol. 22, no. 12, pp. 988–995, 2016.
- [4] P. Zamani *et al.*, "Reflection magnitude as a predictor of mortality the multi-ethnic study of atherosclerosis," *Hypertension*, vol. 64, no. 5, pp. 958–964, 2014.
- [5] M. E. Safar, "Arterial stiffness as a risk factor for clinical hypertension," *Nat. Rev. Cardiol.*, vol. 15, no. 2, pp. 97–105, 2018.
- [6] A. D. Hughes *et al.*, "Limitations of Augmentation Index in the Assessment of Wave Reflection in Normotensive Healthy Individuals," *PLoS One*, vol. 8, no. 3, pp. 1–8, 2013.
- [7] N. Westerhof, P. Sipkema, G. C. V. Den Bos, and G. Elzinga, "Forward and backward waves in the arterial system," *Cardiovasc. Res.*, vol. 6, no. 6, pp. 648–656, 1972.
- [8] C. J. H. Jones and K. H. Parker, "Forward and Backward Running Waves in the Arteries: Analysis Using the Method of Characteristics," *Trans. ASME*, vol. 112, no. 322–326, 1990.
- [9] K. H. Parker, "An introduction to wave intensity analysis," *Med. Biol. Eng. Comput.*, vol. 47, no. 2, pp. 175–188, 2009.
- [10] A. P. G. Hoeks, J. M. Willigers, and R. S. Reneman, "Effects of assessment and processing techniques on the shape of arterial pressure-distension loops," *J. Vasc. Res.*, vol. 37, no. 6, pp. 494–500, 2000.
- [11] R. Manoj, R. Kiran, P. M. Nabeel, J. Joseph, and M. Sivaprakasam, "A Bi-modal Probe Integrated with A-mode Ultrasound and Force Sensor for Single-site Assessment of Arterial Pressure-Diameter Loop," in *IEEE Medical Measurements and Applications, MeMeA 2020 - Conference Proceedings*, 2020, pp. 1–6.
- [12] B. E. Westerhof, I. Guelen, N. Westerhof, J. M. Karemaker, and A. Avolio, "Quantification of wave reflection in the human aorta from pressure alone: A proof of principle," *Hypertension*, vol. 48, no. 4, pp. 595–601, 2006.
- [13] B. Hametner *et al.*, "Wave reflection quantification based on pressure waveforms alone-methods, comparison, and clinical covariates," *Comput. Methods Programs Biomed.*, vol. 109, no. 3, pp. 250–259, 2013.
- [14] J. G. Kips *et al.*, "Evaluation of noninvasive methods to assess wave reflection and pulse transit time from the pressure waveform alone," *Hypertension*, vol. 53, no. 2, pp. 142–149, 2009.
- [15] A. K. Sahani, J. Joseph, R. Radhakrishnan, and M. Sivaprakasam, "Automatic measurement of end-diastolic arterial lumen diameter in ARTSENS," *J. Med. Devices, Trans. ASME*, vol. 9, no. 4, Aug. 2015.
- [16] A. K. Sahani, J. Joseph, and M. Sivaprakasam, "Automated system for imageless evaluation of arterial compliance," *Proc. Annu. Int. Conf. IEEE Eng. Med. Biol. Soc. EMBS*, pp. 227–231, 2012.
- [17] S. Laxminarayan, "The calculation of forward and backward waves in the arterial system," *Med. Biol. Eng. Comput.*, vol. 17, no. 1, p. 130, 1979.
- [18] R. Manoj, V. Raj Kiran, P. M. Nabeel, M. Sivaprakasam, and J. Joseph, "Separation of Forward-Backward Waves in the Arterial System using Multi-Gaussian Approach from Single Pulse Waveform," in *Proceedings of the Annual International Conference of the IEEE Engineering in Medicine and Biology Society, EMBS*, 2021, vol. 2021, pp. 5547–5550.
- [19] C. Liu, D. Zheng, A. Murray, and C. Liu, "Modeling carotid and radial artery pulse pressure waveforms by curve fitting with Gaussian functions," *Biomed. Signal Process. Control*, vol. 8, no. 5, pp. 449–454, 2013.
- [20] J. Joseph, P. M. Nabeel, S. R. Rao, R. Venkatachalam, M. I. Shah, and P. Kaur, "Assessment of Carotid Arterial Stiffness in Community Settings with ARTSENS®," *IEEE J. Transl. Eng. Heal. Med.*, vol. 9, no. November 2020, 2021.
- [21] J. Joseph *et al.*, "ARTSENS® Pen - Portable easy-to-use device for carotid stiffness measurement: Technology validation and clinical-utility assessment," *Biomed. Phys. Eng. Express*, vol. 7, no. 2, 2020.
- [22] J. Joseph, R. Radhakrishnan, S. Kusmakar, A. S. Thrivikraman, and M. Sivaprakasam, "Technical Validation of ARTSENS-An Image Free Device for Evaluation of Vascular Stiffness," *IEEE J. Transl. Eng. Heal. Med.*, vol. 3, no. April, p. 1900213, 2015.
- [23] J. M. Meinders and A. P. G. Hoeks, "Simultaneous assessment of diameter and pressure waveforms in the carotid artery," *Ultrasound Med. Biol.*, vol. 30, no. 2, pp. 147–154, 2004.
- [24] G. F. Mitchell *et al.*, "Changes in arterial stiffness and wave reflection with advancing age in healthy men and women: The Framingham Heart Study," *Hypertension*, vol. 43, no. 6, pp. 1239–1245, 2004.
- [25] C. Fortier and M. Agharazii, "Arterial Stiffness Gradient," *Pulse*, vol. 3, no. 3–4, pp. 159–166, 2015.
- [26] S. S. Hickson *et al.*, "Influence of the central-to-peripheral arterial stiffness gradient on the timing and amplitude of wave reflections," *Hypertens. Res.*, vol. 39, no. 10, pp. 723–729, 2016.
- [27] P. M. Nabeel, J. Joseph, S. Karthik, M. Sivaprakasam, and M. Chenniappan, "Bi-Modal arterial compliance probe for calibration-free cuffless blood pressure estimation," *IEEE Trans. Biomed. Eng.*, vol. 65, no. 11, pp. 2392–2404, 2018.
- [28] P. M. Nabeel, J. Joseph, and M. Sivaprakasam, "A Magnetic Plethysmograph Probe for Local Pulse Wave Velocity Measurement," *IEEE Trans. Biomed. Circuits Syst.*, vol. 11, no. 5, pp. 1065–1076, 2017.
- [29] P. M. Nabeel, J. Joseph, and M. Sivaprakasam, "Variation in local pulse wave velocity over the cardiac cycle: in-vivo validation using dual-MPG arterial compliance probe," *13th Russ. Conf. Biomed. Eng.*, pp. 100–103, 2018.
- [30] S. P. Preejith, R. Dhinesh, J. Joseph, and M. Sivaprakasam, "Wearable ECG platform for continuous cardiac monitoring," *Annu. Int. Conf. IEEE Eng. Med. Biol. Soc. IEEE Eng. Med. Biol. Soc. Annu. Int. Conf.*, vol. 2016, pp. 623–626, Oct. 2016.
- [31] B. Murugesan *et al.*, "ECGNet: Deep Network for Arrhythmia Classification," in *MeMeA 2018 - 2018 IEEE International Symposium on Medical Measurements and Applications, Proceedings*, 2018.
- [32] S. P. Preejith, A. Alex, J. Joseph, and M. Sivaprakasam, "Design, development and clinical validation of a wrist-based optical heart rate monitor," *2016 IEEE Int. Symp. Med. Meas. Appl. MeMeA 2016 - Proc.*, Aug. 2016.
- [33] V. Ravichandran *et al.*, "RespNet: A deep learning model for extraction of respiration from photoplethysmogram," in *Proceedings of the Annual International Conference of the IEEE Engineering in Medicine and Biology Society, EMBS*, 2019, pp. 5556–5559.
- [34] S. P. Preejith, A. Jeelani, P. Maniyar, J. Joseph, and M. Sivaprakasam, "Accelerometer based system for continuous respiratory rate monitoring," *2017 IEEE Int. Symp. Med. Meas. Appl. MeMeA 2017 - Proc.*, pp. 171–176, Jul. 2017.